

Localization and Mapping of Sparse Geologic Features with Unpiloted Aircraft Systems

Zhiang Chen, Sarah Bearman, J Ramón Arrowsmith, Jnaneshwar Das

Abstract— Robotic mapping is attractive in many science applications that involve environmental surveys. This paper presents a system for localization and mapping of sparsely distributed surface features such as precariously balanced rocks (PBRs), whose geometric fragility (stability) parameters provide valuable information on earthquake processes. With geomorphology as the test domain, we carry out a lawnmower search pattern using an Unpiloted Aerial Vehicle (UAV) equipped with a GPS module, stereo camera, and onboard computers. Once a target is detected by a deep neural network, we track its bounding box in the image coordinates by applying a Kalman filter that fuses the deep learning detection with KLT tracking. The target is localized in world coordinates using depth filtering where a set of 3D points are filtered by object bounding boxes from different camera perspectives. The 3D points also provide a strong prior on target shape, which is used for UAV path planning to accurately map the target using RGBD SLAM. After target mapping, the UAS resumes the lawnmower search pattern to locate the next target. Our end goal is a real-time mapping methodology for sparsely distributed surface features on earth or on extraterrestrial surfaces.

I. INTRODUCTION

Although topological mapping using Unpiloted Aerial Systems (UAS) and Structure from Motion (SfM) has recently proliferated in large-scale terrain mapping, UAS-SfM methods are not ideal when targets of interest are sparsely distributed. This is because UAS-SfM methods based on bundle adjustment require intensive offboard computation to produce dense terrain maps that include both targets of interest and other irrelevant features. As the sparsity of targets increases, significant amounts of computation and memory storage are wasted on reconstructing irrelevant features. Additionally, UAS-SfM methods like offboard mapping decouple robot navigation from mapping. This inhibits adaptive or active mapping that can optimize flight paths to locate and map specific targets.

Target localization is a process of estimating a target's location in 3D space. Previously, target location was simplified by determining the target's geometric center, which is useful when the target's dimensions are negligible. However, in scenarios where the target's dimensions matter, a representation of the target's location that includes its geometric information is desired. In this work, a target's location is represented by a set of 3D points, which can indicate its geometric center, orientation, and dimension. This additional information facilitates UAV path planning for target mapping.

Authors are affiliated with the School of Earth and Space Exploration, Arizona State University, 781 Terrace Mall, Tempe, AZ 85287, USA

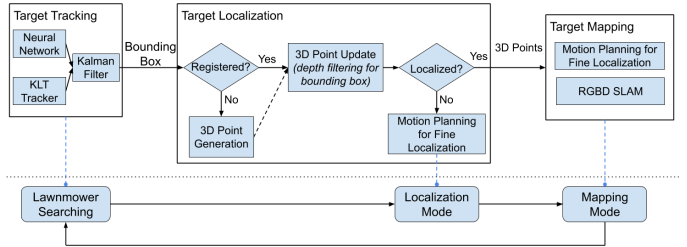


Fig. 1. System workflow. The system includes target tracking, target localization, and target mapping. The motion mode switches from lawnmower searching during target tracking to localization mode once fine localization is requested, and then switches to mapping mode after the target is finely localized.

This work is motivated by the challenges of finding and mapping precariously balanced rocks (PBRs). PBRs are easily toppled by strong earthquake shaking, so their existence can provide valuable information about earthquake history in a given region. Previous work has focused on PBR's geometric models and dynamic models interacting with ground motion [1]. However, model assessment in a large, statistical scene is barely researched because PBRs are sparsely distributed and difficult to identify, which makes it challenging to find and map them.

The goal of this paper is to present an efficient, real-time approach to localize and map sparse targets by taking advantage of deep neural network object detection, sample-based state estimation, and RGBD SLAM. The system workflow is shown in Fig. 1. We start by tracking bounding box coordinates in image frames using a Kalman filter that fuses deep neural network detection and KLT tracking. Then, the target is localized in world coordinates by sampling a set of 3D points that are generated by back projecting a polyhedral cone from the vertices of the enlarged tracked bounding box at different camera perspectives. Finally, we deploy RGBD SLAM for accurate target mapping.

II. TARGET TRACKING

We employ a deep neural network to detect targets, and then track their bounding boxes in image coordinates using a Kalman filter. A KLT tracker is used to predict the new state of each bounding box, and the state variable is updated using object detection from the deep neural network. We use an IoU threshold to register new bounding boxes, and we deregister the bounding boxes when they move out of the current image frame. False detections are deregistered by utilizing the differential entropy of bounding box state distributions.

The Kalman filter algorithm is presented in Algorithm 1. The state variable of the Kalman filter is the bounding box coordinates $\mathbf{x} = (u_{min}, v_{min}, 1, u_{max}, v_{max}, 1)$ in homogeneous coordinate system, or $\mathbf{u} = (u_{min}, v_{min}, u_{max}, v_{max})$ in Euclidean coordinate system. Homogeneous coordinate system and Euclidean coordinate system can be converted by matrix operations:

$$\mathbf{x}_{t-1} = \mathbf{T}\mathbf{u}_{t-1} + \mathbf{a}$$

$$\mathbf{u}_t = \mathbf{M}\mathbf{x}_t$$

where

$$\mathbf{T} = \begin{bmatrix} 1 & 0 & 0 & 0 \\ 0 & 1 & 0 & 0 \\ 0 & 0 & 0 & 0 \\ 0 & 0 & 1 & 0 \\ 0 & 0 & 0 & 1 \\ 0 & 0 & 0 & 0 \end{bmatrix}, \mathbf{a} = \begin{bmatrix} 0 \\ 0 \\ 1 \\ 0 \\ 0 \\ 1 \end{bmatrix}, \mathbf{M} = \begin{bmatrix} 1 & 0 & 0 & 0 & 0 & 0 \\ 0 & 1 & 0 & 0 & 0 & 0 \\ 0 & 0 & 0 & 1 & 0 & 0 \\ 0 & 0 & 0 & 0 & 1 & 0 \end{bmatrix}$$

Lines 1-2 and Lines 5-6 in Algorithm show the conversions between homogeneous and Euclidean coordinates.

The predict phase uses a KLT tracker to estimate a bounding box state. We consider a linear prediction model for bounding boxes,

$$\mathbf{x}_t = \mathbf{F}_{t-1}\mathbf{x}_{t-1} + \mathbf{e}_{t-1} \quad (1)$$

where $\mathbf{F}_{6 \times 6}$ is state transition model, and $\mathbf{e} \in \mathbb{R}^6$ is a prediction error vector:

$$\mathbf{F} = \begin{bmatrix} \mathbf{S} & \mathbf{0} \\ \mathbf{0} & \mathbf{S} \end{bmatrix}, \mathbf{e} = (e, e, 0, e, e, 0)$$

$\mathbf{S}_{3 \times 3}$ is a similarity transform produced from KLT tracker that applies Harris features in the bounding box. We use homogeneous coordinate system in the predict phase to keep consistent with \mathbf{F} , which is in 2D homogeneous coordinates.

Object detection from the deep neural network is employed to update the state variable,

$$\mathbf{z}_t = \mathbf{H}\mathbf{u}_t + \mathbf{w}_t \quad (2)$$

where $\mathbf{H}_{4 \times 4}$ is an identity matrix, $\mathbf{w} \in \mathbb{R}^4$ is an error vector for the updating model, and $\mathbf{z} = (u_{min}, v_{min}, u_{max}, v_{max}) \in \mathbb{R}^4$ is bounding box coordinates from the neural network. We obtain these coordinates from

$$\mathbf{z}_t = f(I_t) \quad (3)$$

where I is an input image and f is an object detection neural network. We assume both predict error \mathbf{e} and update error \mathbf{w} have multi-variable Gaussian distribution:

$$\mathbf{e} \sim \mathcal{N}(\mathbf{0}, \mathbf{R}), \mathbf{w} \sim \mathcal{N}(\mathbf{0}, \mathbf{Q})$$

where $\mathbf{R}_{6 \times 6}$, $\mathbf{Q}_{4 \times 4}$ are the covariance matrices:

$$\mathbf{R} = \begin{bmatrix} e^2 & 0 & 0 & 0 & 0 & 0 \\ 0 & e^2 & 0 & 0 & 0 & 0 \\ 0 & 0 & 0 & 0 & 0 & 0 \\ 0 & 0 & 0 & e^2 & 0 & 0 \\ 0 & 0 & 0 & 0 & e^2 & 0 \\ 0 & 0 & 0 & 0 & 0 & 0 \end{bmatrix}, \mathbf{Q} = w^2 \mathbf{I}_{4 \times 4}$$

Algorithm 1 Kalman Filter for Bounding Box Tracking

input: $\mathbf{u}_{t-1}, \Sigma_{t-1}, \mathbf{F}_{t-1}, \mathbf{z}_t$

output: \mathbf{u}_t

parameter: \mathbf{R}, \mathbf{Q}

Predict:

1. $\mathbf{x}_{t-1} = \mathbf{T}\mathbf{u}_{t-1} + \mathbf{a}$
2. $\Omega_{t-1} = \mathbf{T}\Sigma_{t-1}\mathbf{T}^T + \mathbf{a}\mathbf{a}^T$
3. $\mathbf{x}_t = \mathbf{F}_{t-1}\mathbf{x}_{t-1}$
4. $\Omega_t = \mathbf{F}_{t-1}\Omega_{t-1}\mathbf{F}_{t-1}^T + \mathbf{R}$
5. $\mathbf{u}_t = \mathbf{M}\mathbf{x}_t$
6. $\Sigma_t = \mathbf{M}\Omega_t\mathbf{M}^T$

Update:

7. $\mathbf{K} = \Sigma_t(\Sigma_t + \mathbf{Q})^{-1}$
8. $\mathbf{u}_t = \mathbf{u}_t + \mathbf{K}(\mathbf{z}_t - \mathbf{u}_t)$
9. $\Sigma_t = (\mathbf{I}_{4 \times 4} - \mathbf{K})\Sigma_t$

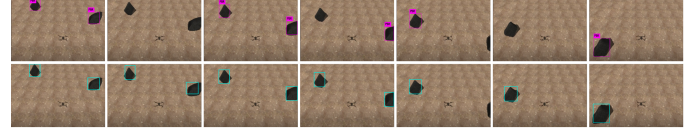


Fig. 2. Kalman filtering for bounding box tracking. The UAV is moving north. The top-row images are neural network detection. The bottom-row images are the results for the Kalman-filtering tracking.

and $\mathbf{I}_{4 \times 4}$ is an identity matrix. We use Euclidean coordinate system in the update phase because an invertible covariance matrix is needed to update Kalman gain \mathbf{K} , while the covariance matrix in homogeneous coordinate system Ω is degenerate.

A new bounding box detected from the neural network will be registered if its IoU is smaller than a threshold of 0.3 with any previously registered bounding boxes. Otherwise, the new bounding box coordinates will be used to update the registered bounding boxes that satisfy the IoU threshold. A bounding box will be deregistered when it is moving out of the current image frame.

False detection from the deep neural network can be problematic, so we record the differential entropy of each bounding-box-state distribution:

$$h = \frac{k}{2} + \frac{k}{2} \ln(2\pi) + \frac{1}{2} \ln(|\Sigma|) \quad (4)$$

where $k = 4$ is the dimensionality of the state vector space. When the differential entropy h becomes greater than a threshold of 16, it implies there has been no update for several predictions and the bounding box will be deregistered. The tracking result is shown in Fig. 2.

III. TARGET LOCALIZATION

Once a target is tracked in image frames, we randomly generate 3D points within a four-face polyhedral cone that is back-projected from an enlarged bounding box (Fig. 3(A)). The 3D points will be projected to different image frames and resampled according to their positions with respect to the tracked bounding box (Fig. 3(B)). The rationale is similar to the depth filter in [2], but we adapt it to bounding boxes and use a set of 3D points to represent a target location.

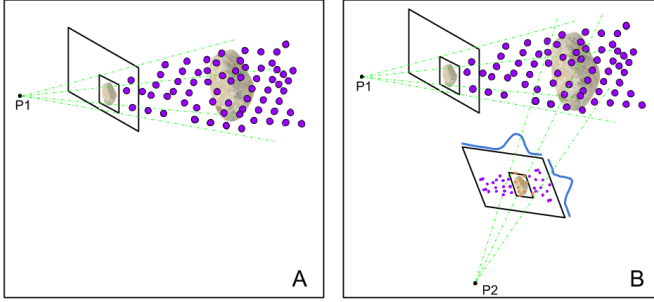


Fig. 3. 3D point generation and update. (A) 3D points are generated within a polyhedral cone that are back-projected from an enlarged bounding box. (B) The 3D points are projected to a different image frame and resampled according to their projections' positions with respect to the new bounding box.

Unlike previous work that simplifies target locations as geometric centers, 3D points offer added information such as orientation and dimension, which can facilitate UAV motion planning for target mapping.

A. Camera Model

We derive the back-projection of image points to rays on special Euclidean group based on the models in Hartley and Zisserman's book [3]. A general projective camera maps a point in space $\mathbf{L} = (x, y, z, 1)$ to an image point $\mathbf{l} = (u, v, 1)$ according to the mapping $\mathbf{l} = \mathbf{PL}$. \mathbf{P} is the projection matrix, and $\mathbf{P} = [K|\mathbf{0}]T_c^w$, where $K_{3 \times 3}$ is the camera intrinsic matrix, and $T_c^w \in SE(3)$ is the transformation matrix from world frame to camera frame. We can back-project a ray from an image point,

$$\mathbf{r}_c = S(\mu K^{-1}\mathbf{l}) + \mathbf{b} \quad (5)$$

$$\mathbf{r}_w = T_w^c \mathbf{r}_c \quad (6)$$

where \mathbf{r}_c is a homogeneous 3D point in camera frame, \mathbf{r}_w is a homogeneous 3D point in world frame, μ is a non-negative scalar, $S_{4 \times 3} = \begin{bmatrix} I_{3 \times 3} \\ \mathbf{0} \end{bmatrix}$, $\mathbf{b} = (0, 0, 0, 1)$, and $T_w^c \in SE(3)$ is the transformation matrix from camera frame to world frame. S and \mathbf{b} convert Euclidean coordinates to Homogeneous coordinates. A ray in world frame is represented by a 3D point set $\eta = \{\mathbf{r}_w | \mu \geq 0\}$.

B. 3D Point Generation

We have $T_w^c = T_w^b T_b^c$, where T_b^c is the transformation matrix from camera frame to robot base frame, and T_w^b is the transformation matrix from robot base frame to world frame. We enlarge bounding boxes from target tracking to account for errors in the drone state estimator. A four-face polyhedral cone, $\{\eta_{w1}, \eta_{w2}, \eta_{w3}, \eta_{w4}\}$, is generated by four 3D rays back-projected from four corners of the enlarged bounding box. To randomly initialize a 3D point in the cone, we adopt the following steps.

- 1) randomly generate a direction vector from a convex combination of four enlarged corner vectors:

$$\mathbf{v} = \alpha_1 K^{-1}\mathbf{l}_1 + \alpha_2 K^{-1}\mathbf{l}_2 + \alpha_3 K^{-1}\mathbf{l}_3 + \alpha_4 K^{-1}\mathbf{l}_4 \quad (7)$$

Algorithm 2 3D Point generation

input: $\{\mathbf{l}_1, \mathbf{l}_2, \mathbf{l}_3, \mathbf{l}_4\}, m, T_w^c$

output: P_w

parameter: K, d_m

1. $A = \mathbb{U}(4, m)$
2. $B = Diag(|A|_m)$
3. $\tilde{A} = AB^{-1}$
4. $C = [K^{-1}\mathbf{l}_1, K^{-1}\mathbf{l}_2, K^{-1}\mathbf{l}_3, K^{-1}\mathbf{l}_4]$
5. $\delta = d_m \mathbb{U}(1, m)$
6. $\tilde{\delta} = Diag(\delta)$
7. $\tilde{P}_c = C\tilde{A}\tilde{\delta}$
8. $P_c = S\tilde{P}_c + \mathbf{b}$
9. $P_w = T_w^c P_c$

Comments:

- 1). m is the number of 3D points to be generated.
- 2). $\mathbb{U}(x, y)$ is a standard uniform sampler returning a $x \times y$ matrix.
- 3). $Diag(x)$ creates a diagonal matrix from a vector x .
- 4). $|\cdot|_m$ returns a vector of Manhattan distances of all columns.
- 5). d_m is the maximum depth of 3D points along z axis in camera frame.

s.t.

$$\alpha_1, \alpha_2, \alpha_3, \alpha_4 \sim \mathcal{U}$$

$$\alpha_1 + \alpha_2 + \alpha_3 + \alpha_4 = 1$$

where \mathcal{U} is a standard uniform distribution.

- 2) randomly scale the direction vector: $\tilde{\mathbf{L}} = \delta \mathbf{v}$, where δ is a random depth. $\tilde{\mathbf{L}}$ is a Homogeneous 3D point in the cone in camera frame.
- 3) convert the 3D point to world frame: $\mathbf{L} = T_w^c(S\tilde{\mathbf{L}} + \mathbf{b})$. \mathbf{L} is one randomly generated point in world frame. We generate 1000 3D points to localize a tracked target using the matrix form of 3D point generation in Algorithm 2.

When a bounding box is updated in tracking, a new set of 3D points will be generated when there is no existing 3D point in the cone back-projected from the updated bounding box. A four-face polyhedral cone from a bounding box can be represented by four inward half-spaces. For convenience, we use camera frame for 3D point registration because all four hyperplanes pass through the origin. Then we have a 3D point registration condition:

$$\mathbf{N}\tilde{\mathbf{L}} > \mathbf{0} \quad (8)$$

where $\tilde{\mathbf{L}} = (x, y, z)$ is the 3D point in camera frame, $\mathbf{N}_{4 \times 3}$ is composed of four rows of positive normal vectors on the four half-spaces. Positive normal vectors on a half-space can be acquired by cross product, $\mathbf{n}_{ij} = (K^{-1}\mathbf{l}_i) \times (K^{-1}\mathbf{l}_j)$, where $\mathbf{l}_i, \mathbf{l}_j$ are two adjacent enlarged corners in clockwise order. If there is no existing 3D point satisfying the condition, a new set of 3D points will be registered; otherwise, the set of registered 3D points that consist of any points satisfying the condition will be updated.

C. 3D Point update

Our 3D point update is adapted from the depth filter in SVO [2] and developed for semantic bounding box localization. We project existing 3D points to new image frames and resample them based on the positions between their projections and the bounding boxes in the new frames

Algorithm 3 3D Point Update

input: P_w , \mathbf{x} , T_c^w
output: P'_w
parameter: σ , m , K

1. $\mathbf{a} = \sqrt{\sigma} \mathbb{N}(m, 3)$
2. $\bar{\mathbf{a}} = \mathbf{S}\mathbf{a} + \mathbf{b}$
3. $\mathbf{p} = [K|\mathbf{0}|T_c^w(P_w + \bar{\mathbf{a}})]$
4. $\mathbf{i} = f(\mathbf{p}|\mathbf{x})$
5. $P'_w = \text{Importance_Sampling}(P_w, \mathbf{i})$

Comments:

- 1). $\mathbb{N}(x, y)$ is an isotropic standard multi-variate Gaussian sampler returning a $x \times y$ matrix.
- 2). $\sqrt{\sigma}$ is the standard variance of update noise.
- 3). $f(\mathbf{p}|\mathbf{x})$ is a two-variable distribution composed of a Gaussian distribution and a uniform distribution.

(Algorithm 3). The distribution $f(\mathbf{p}|\mathbf{x})$ assesses the weights of image points \mathbf{p} given a bounding box \mathbf{x} , and is formed by a summation of a Gaussian distribution and a uniform distribution:

$$f(\mathbf{p}|\mathbf{x}) = w_1 h(\mathbf{p}|\mathbf{x}) + w_2 g(\mathbf{p}|\mathbf{x}) \quad (9)$$

where $h(\mathbf{p}|\mathbf{x})$ is distribution density function of a 2D Gaussian distribution $\mathcal{N}(\mathbf{c}_x, \Sigma_x)$, and $g(\mathbf{p}|\mathbf{x})$ is distribution density function of a 2D uniform distribution \mathcal{U} among an enlarged area of the bounding box \mathbf{x} . Variables w_1 and w_2 are the weights of the two distributions. For $\mathcal{N}(\mathbf{c}_x, \Sigma_x)$,

$$\mathbf{c}_x = \left(\frac{u_{min} + u_{max}}{2}, \frac{v_{min} + v_{max}}{2} \right), \Sigma_x = \begin{bmatrix} \left(\frac{u_{max} - u_{min}}{2} \right)^2 & 0 \\ 0 & \left(\frac{v_{max} - v_{min}}{2} \right)^2 \end{bmatrix}$$

The 3D points P_w in Algorithm 3 will be resampled according to their weights from the joint distribution by importance sampling.

D. Properties

Some properties are used to describe 3D points and determine if localization has been achieved. We apply Principle Component Analysis to each 3D point set. The largest eigenvalue λ_m can indicate how a 3D point set is converged. We also utilize the eigenvalues and eigenvectors to approximate an ellipsoid, which can be used for visualization and to convey target orientation information.

When a 3D point set has been updated, we want to measure the amount of information gain from the update. One metric that captures relative entropy is Kullback–Leibler divergence (KL divergence) of updated 3D point distribution with respect to previous 3D point distribution. To compute KL divergence, we estimate the 3D point set with a three-dimensional Gaussian distribution, whose mean and covariance are approximated by the mean and covariance of the 3D points. We can compute the KL divergence following the formula for multivariate Gaussian distribution:

$$D_{KL}(\mathcal{N}_0 || \mathcal{N}_1) = \frac{1}{2} (tr(\Pi_1^{-1} \Pi_0) + (\tau_1 - \tau_0)^T \Pi_1^{-1} (\tau_1 - \tau_0) - k + \ln(\frac{|\Pi_1|}{|\Pi_0|})) \quad (10)$$

where $k = 3$ is the dimension of the random variable, $\mathcal{N}_0(\tau_0, \Pi_0)$ is the estimated Gaussian distribution of the

updated 3D points, $\mathcal{N}_1(\tau_1, \Pi_1)$ is the estimated Gaussian distribution of the previous 3D points, and $tr(\cdot)$ is a matrix trace function.

Similar to bounding box tracking, we also inspect differential entropy of each 3D point set h_p . In the case of multivariate Gaussian distribution approximation as stated above, the differential entropy shows the compactness of a 3D point set.

Since we have no prior knowledge of targets and the state estimator is not precise, it is challenging to find a sufficient condition for localization. In practice, we jointly consider the necessary conditions such as the largest eigenvalue λ_m , KL divergence $D_{KL}(\mathcal{N}_0 || \mathcal{N}_1)$, and differential entropy h_p to decide the status of target localization. λ_m should be smaller than a threshold. When 3D points are converged, any new update will not change the 3D point distribution, and the 3D points should be compact. Thus we also need thresholds for $D_{KL}(\mathcal{N}_0 || \mathcal{N}_1)$ and h_p .

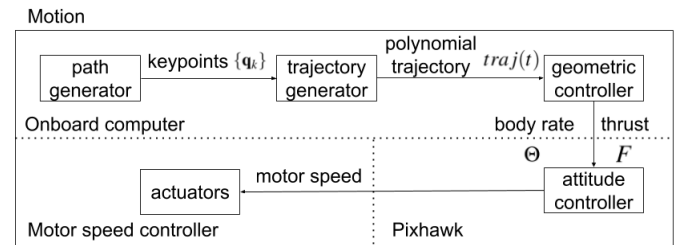


Fig. 4. UAV motion system.

E. Motion Planning

We need multiple, different camera perspectives with bounding boxes to localize a target. A view planning is necessary especially when there are large noises in T_c^w and \mathbf{x} . A lawn mower flight pattern is initialized to search targets of interest. Once a set of 3D points has a largest eigenvalue λ_m and a differential entropy h_p that are smaller than certain thresholds but not small enough to accurately localize the target due to the lack of enough camera perspectives, we deploy a motion planning for fine localization. The sketch of the motion planning is presented in Fig. 5.

We approach the motion planning problem by first considering constraints and then finding a feasible solution. We want to have only one motion system in target search, fine localization and mapping. The motion system is shown in Fig. 4. The trajectory generator uses keypoints from the path generator to minimize the snap of 10th-degree polynomials [4]. The geometric controller [5] [6] takes a desired robot's position and yaw heading and outputs desired robot's body rate and thrust. In the target search stage, the path generator is a hard-coding lawn mower pattern. For fine localization, the path generator should produce a set of keypoints, e.g. a set of robot poses $\{q_k\}$ such that the sequential controllers can generate camera perspectives to reduce uncertainty in the target location. Since the geometric controller only deal with desired position and yaw, we add maximum acceleration and

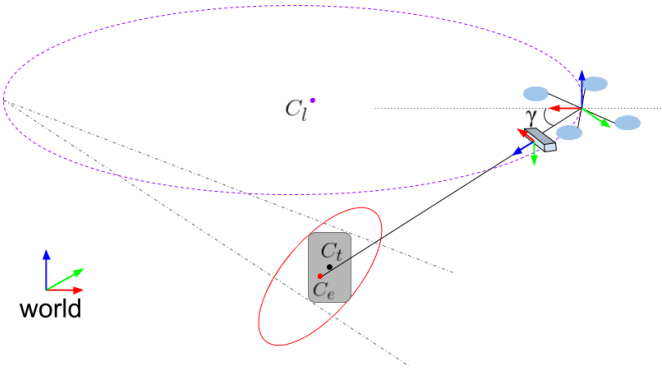


Fig. 5. Path planning for fine localization. The ellipse at the bottom represents a sideview of the ellipsoid from PCA. $C_e = (x_e, y_e, z_e)$ is the center of the ellipsoid. The dark-gray rounded rectangle represents a target with the center C_t . The large ellipse on the top is the circular path with the center $C_l = (x_e, y_e, h_s)$. γ is the angle between the camera z axis and the horizontal plane.

maximum velocity constraints in trajectory generator so that UAV's pose can be approximated to hovering pose. That is, UAV's roll and pitch angles will be negligible to affect the target projections in images. For view planning, we simply consider hovering pose without handling UAV dynamics. Since the distance d_1 between C_e and the camera is much larger than the distance d_2 between the camera to the UAV ($d_1 : d_2 > 10 : 1$), we do not distinguish them in the motion planning.

We constrain the UAV positions on the horizontal plane that is parallel to XY plane in world frame and has the same height as the lawn mower search height h_s . There are four variables to be determined $(x, y, \text{yaw}, \gamma)$, where (x, y) is the UAV coordinates on the horizontal plane in world frame, yaw is the UAV's heading, and γ is the angle between the camera z axis and the horizontal plane (Fig. 5). Since we use the 3D points information from rough localization to decide a view planning and the rough localization is not accurate, the 3D points projection in the image can deviate from the actual target projection. To alleviate this issue, we set the camera z axis passing through the 3D point center (mean Euclidean distance) C_e to keep the target projection in image frame as much as possible.

We decide the next-best-view to have the camera z axis aligning with the eigenvector with the smallest eigenvalue (smallest eigenvector). That is, the image plane is parallel to the plane formed by the eigenvectors with the largest and the second largest values, which is the plane with the largest uncertainty. From such camera pose, the bounding box on the image plane can reduce most uncertainty in the 3D points.

However, when the smallest eigenvector is parallel to the horizontal plane, the next best view will be at infinity and $\gamma \rightarrow 0$. We relax the optimality by having a fix angle γ between the camera z axis and the horizontal plane and minimizing the angle between camera z axis and the smallest eigenvector. By having a fix angle γ , the left two variables (x, y) will be constrained by a circle $C_l : (x - x_e)^2 + (y -$

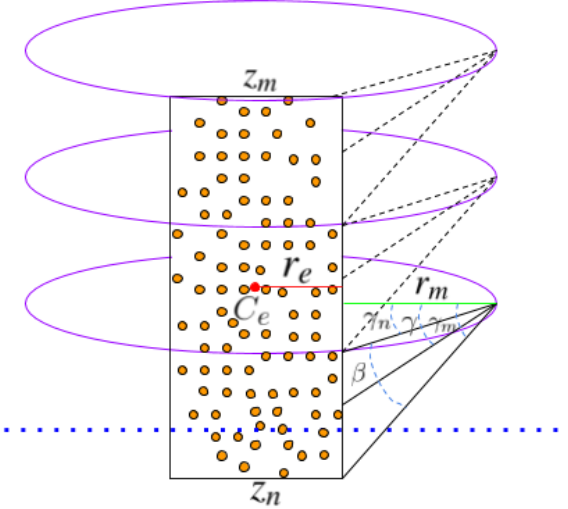


Fig. 6. Path planning for mapping. The small yellow dots represent 3D points for a target. C_e is the center of the 3D points (mean Euclidean distance). r_e is the radius of the cylinder. r_m is the altitude of the cylinder top. r_n is the altitude bottom. r_m is the distance to be kept between the UAV and the cylinder. β is the vertical scanning angle between the upper scanning ray and the lower scanning ray. The vertical scanning β is similar to the camera vertical field of view but has a smaller angle. The three circles are the planned path for this case. γ_m is the lower scanning angle $\gamma_m = \gamma - \frac{\beta}{2}$. γ_h is the upper scanning angle $\gamma_h = \gamma + \frac{\beta}{2}$.

$y_e)^2 = \frac{(h_s - z_e)^2}{\tan^2(\gamma)}$. Due to the ambiguity of eigenvector direction, we set the smallest eigenvector to have a non-negative value along z world axis v_z . In other words, if the smallest eigenvector has negative v_z , we flip the direction. When $v_z > 0$, the solution of the minimization is the intersection between the circle and the eigenvector projection on the circle plane. When $v_z = 0$, we set the next-best-view point on the circle as the farthest point to the current UAV position. We add a circular path to connect the current UAV pose and the next-best-view pose. The start keypoint is current UAV pose. The next keypoint is the closest point on the circle C_l . Then the UAV will follow the circle curve C_l to approach the next-best-view pose and the heading is always toward the 3D points center C_e .

IV. TARGET MAPPING

We deploy an RGBD SLAM [7] for target mapping after fine localization. We use the same motion system for search and fine localization, except that the keypoints from the path generator should present enough camera views to map the full-body of a target. The 3D points from the fine localization provide occupancy information of a target, which is exploited to plan a path for the mapping. We apply a circular scanning for this purpose as shown in Fig. 6. We first fit the 3D points with a vertical cylinder: the cylinder's axis traverses the center of the 3D points C_e , its top is at the highest 3D point, its bottom is at the lowest 3D point, and its radius is the smallest radius that can include all 3D points. One objective of the path planning is to provide enough camera views to determine the occupancy uncertainty of the space

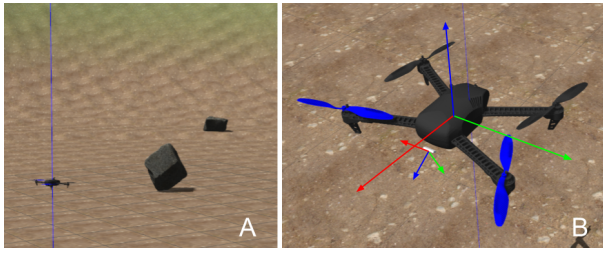


Fig. 7. Gazebo simulation. (A) boulder world. (B) 3DR Iris with RGBD sensor.

around the cylinder.

We deploy a circular path for the mapping, which can produce a 360-degree scan of the target (Fig. 6). The circles lie on horizontal planes that are parallel to XY plane in world frame. The centers of the circles are on the axis of the cylinder. We set the circle radius $r_c = r_e + r_m$ to keep some distance between the UAV and the cylinder. The heights and number of the circles are decided by the camera mount angle γ and vertical scanning angle β (Fig. 6). We have β slightly smaller than the camera vertical field of view so that there are vertical overlaps. The first circle is placed at the bottom where the cylinder bottom can be just covered by the lower scanning ray. The other circles are repeatedly arranged upward until the cylinder top can be covered by an upper scanning ray.

V. EXPERIMENT

We conducted an experiment in Gazebo simulation (Fig. 7) in a gaming laptop (Dell G7: Intel Core i7-8750H, 16GB memory, Nvidia GeForce GTX 1060 Max-Q). We used a 3DR Iris with a RGBD sensor ($\gamma = 55^\circ$) operated by PX4 SITL and MAVROS. YOLO v2 [8] is fine tuned with the images collected in the Gazebo world. The target detection and tracking is shown in Fig. 2.

The maximum velocity is $1m/s$ and the maximum acceleration is $1m/s^2$. The vertical scanning angle is 40° . The result of fine location and mapping is shown in Fig. 8.

VI. FUTURE WORK

The latency in target tracking can cause false 3D point generation issue. We will alleviate this problem by using our target tracking offline to generate more labels and retraining the object detection network. As long as the object detection neural network has high enough detection rate, target tracking can be discarded. Alternatively, we can look at recent research in object tracking neural networks.

The accuracy of fine localization depends on the initial 3D-point distribution. Instead of using importance sampling to update 3D points throughout fine localization, uniform resampling should be applied to promote 3D-point distribution at early stage.

In the fine localization stage, bundle adjustment can be used to jointly improve the accuracy of the target localization and the UAV state estimation.

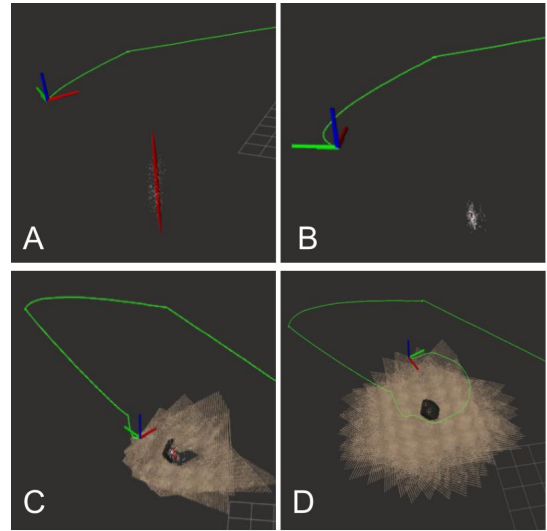


Fig. 8. Localization and mapping. (A, B) target localization. (C, D) target mapping. The vertical ellipsoid in (A) indicates large uncertainty along vertical axis. As the 3D points are converged in (B), motion planning for target mapping is triggered. Then the UAV moves closer to the target and deploys RGBD SLAM.

ACKNOWLEDGEMENTS

This work was supported in part by Southern California Earthquake Center (SCEC) award 20129, and National Science Foundation award CNS-1521617.

REFERENCES

- [1] David E Haddad et al. "Estimating two-dimensional static stabilities and geomorphic settings of precariously balanced rocks from unconstrained digital photographs". In: *Geosphere* 8.5 (2012), pp. 1042–1053.
- [2] Christian Forster, Matia Pizzoli, and Davide Scaramuzza. "SVO: Fast Semi-Direct Monocular Visual Odometry". In: *IEEE International Conference on Robotics and Automation (ICRA)*. 2014.
- [3] Richard Hartley and Andrew Zisserman. *Multiple View Geometry in Computer Vision*. Cambridge university press, 2003.
- [4] Charles Richter, Adam Bry, and Nicholas Roy. "Polynomial trajectory planning for aggressive quadrotor flight in dense indoor environments". In: *Robotics Research*. Springer, 2016, pp. 649–666.
- [5] Jaeyoung Lim. *mavros_controllers - Aggressive trajectory tracking using mavros for PX4 enabled vehicles*. Mar. 2019. DOI: 10.5281/zenodo.2652888. URL: <https://doi.org/10.5281/zenodo.2652888>.
- [6] Taeyoung Lee, Melvin Leok, and N Harris McClamroch. "Geometric tracking control of a quadrotor UAV on SE (3)". In: *49th IEEE conference on decision and control (CDC)*. IEEE. 2010, pp. 5420–5425.

- [7] Mathieu Labb  and Fran ois Michaud. “RTAB-Map as an open-source lidar and visual simultaneous localization and mapping library for large-scale and long-term online operation”. In: *Journal of Field Robotics* 36.2 (2019), pp. 416–446.
- [8] Joseph Redmon and Ali Farhadi. “YOLO9000: better, faster, stronger”. In: *Proceedings of the IEEE conference on computer vision and pattern recognition*. 2017, pp. 7263–7271.